Published in Nature 448, 92-96, 2007
which should be used for any reference to this work

Structural snapshots along the reaction pathway of ferredoxin–thioredoxin reductase

Shaodong Dai[1], Rosmarie Friemann[2]†, Dominique A. Glauser[3]†, Florence Bourquin[3]†, Wanda Manieri[3]†, Peter Schürmann[3] & Hans Eklund[2]

Oxygen-evolving photosynthetic organisms regulate carbon metabolism through a light-dependent redox signalling pathway[1]. Electrons are shuttled from photosystem I by means of ferredoxin (Fdx) to ferredoxin–thioredoxin reductase (FTR), which catalyses the two-electron-reduction of chloroplast thioredoxins (Trxs). These modify target enzyme activities by reduction, regulating carbon flow[2]. FTR is unique in its use of a [4Fe–4S] cluster and a proximal disulphide bridge in the conversion of a light signal into a thiol signal[2]. We determined the structures of FTR in both its one- and its two-electron-reduced intermediate states and of four complexes in the pathway, including the ternary Fdx–FTR–Trx complex. Here we show that, in the first complex (Fdx–FTR) of the pathway, the Fdx [2Fe–2S] cluster is positioned suitably for electron transfer to the FTR [4Fe–4S] centre. After the transfer of one electron, an intermediate is formed in which one sulphur atom of the FTR active site is free to attack a disulphide bridge in Trx and the other sulphur atom forms a fifth ligand for an iron atom in the FTR [4Fe–4S] centre—a unique structure in biology. Fdx then delivers a second electron that cleaves the FTR–Trx heterodisulphide bond, which occurs in the Fdx–FTR–Trx complex. In this structure, the redox centres of the three proteins are aligned to maximize the efficiency of electron transfer from the Fdx [2Fe–2S] cluster to the active-site disulphide of Trxs. These results provide a structural framework for understanding the mechanism of disulphide reduction by an iron–sulphur enzyme[3] and describe previously unknown interaction networks for both Fdx and Trx (refs 4–6).

Fdx provides electrons for regulatory purposes to transmit a light signal from the thylakoid membranes in plants to target enzymes by means of the FTR system (Supplementary Fig. 1)[1]. The FTR cascade begins with the formation of a transient complex between Fdx and FTR (Fig. 1a) and is followed by a straightforward electron transfer from reduced Fdx to FTR (see below; species **1** → **2**).

FTR, found only in oxygenic photosynthetic cells, is a thin, flat, heterodimeric molecule. It contains a catalytic and a variable subunit, and has a width of about 10 Å in the centre of the catalytic subunit where the [4Fe–4S] cluster is located[7]. On one side of the disk-shaped molecule, the redox-active disulphide covers the iron–sulphur centre; on the opposite side, a Cys-*cis*-Pro-Cys (CPC) motif contributes both cysteines to ligate the iron (Fig. 2a). In the structure of the Fdx–FTR complex, Fdx docks at the side of FTR that contains the CPC motif and interacts only with the catalytic subunit. No significant conformational changes in either FTR or Fdx occur when they bind

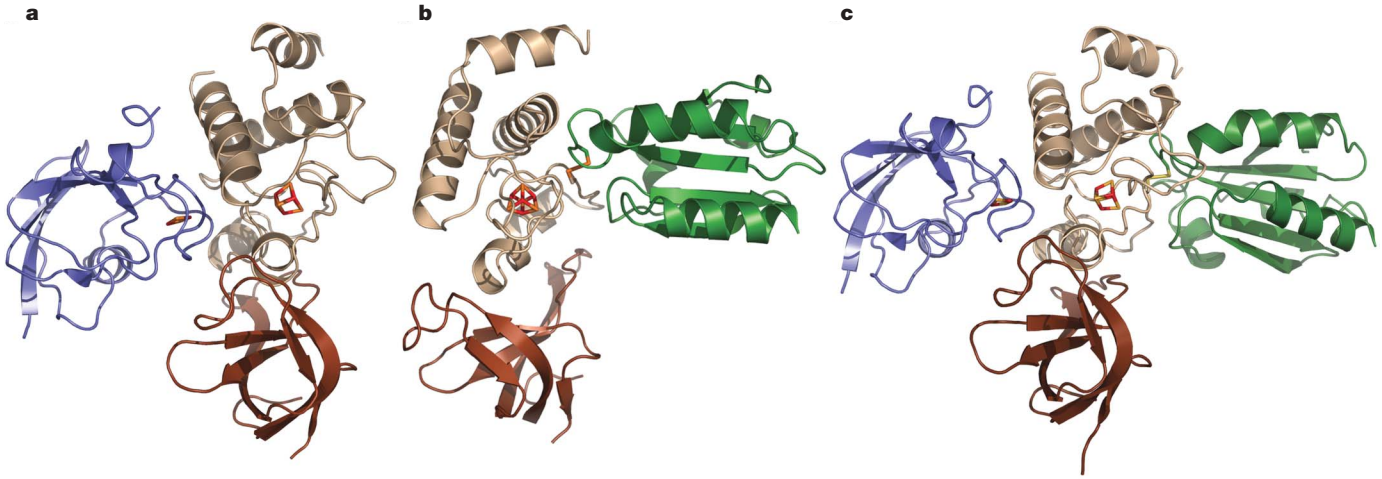

Figure 1 | Overall structures of Fdx–FTR, FTR–Trx-*f*(C49S) and Fdx–FTR–Trx-*f*(C49S) complexes. Fdx, the catalytic subunit of FTR, the variable subunit of FTR and Trx-*f*(C49S) are coloured blue, beige, brown and green, respectively. The [2Fe–2S] cluster of Fdx and [4Fe–4S] cluster of FTR are represented in sticks, where iron and sulphur atoms are coloured red and orange, respectively. **a**, Overall structure of the Fdx–FTR complex. Fdx interacts solely with the catalytic subunit of FTR. **b**, Crystal structure of FTR–Trx-*f*(C49S) complex. Trx-*f* exclusively interacts with the catalytic subunit of FTR. **c**, Structure of the Fdx–FTR–Trx-*f*(C49S) complex.

[1]Howard Hughes Medical Institute, Integrated Department of Immunology, National Jewish Medical and Research Center & University of Colorado Health Sciences Center, 1400 Jackson Street, Denver, Colorado 80206, USA. [2]Department of Molecular Biology, Swedish University of Agricultural Sciences, Biomedical Centre, Box 590, S-75124 Uppsala, Sweden. [3]Université de Neuchâtel, Laboratoire de Biologie Moléculaire et Cellulaire, Rue Emile Argand 11, CH-2009 Neuchâtel, Switzerland. †Present addresses: Department of Chemistry, University of Oslo, PB 1033, Blindern, 0315 Oslo, Norway (R.F.); Fondation pour Recherches Médicales, CH-1211 Genève, Switzerland (D.A.G.); Biochemisches Institut, Universität Zürich, CH-8057 Zürich, Switzerland (F.B.); College of Pharmacy, Medical Center, University of Cincinnati, Cincinnati, Ohio 45267-0004, USA (W.M.).

each other[7–9]. The shortest distance between the edges of the iron–sulphur centres of the two proteins is about 11 Å. Although electron transfer through space would, at this distance, be possible, it would be appreciably faster through a hydrogen- and covalent-bonded pathway[10]. Such a pathway probably exists, because Ser 38 of Fdx forms a hydrogen bond to the carbonyl oxygen of Cys 74 in the FTR CPC motif, providing a short connection between the [2Fe–2S] cluster of Fdx and the [4Fe–4S] cluster of FTR (Supplementary Fig. 2).

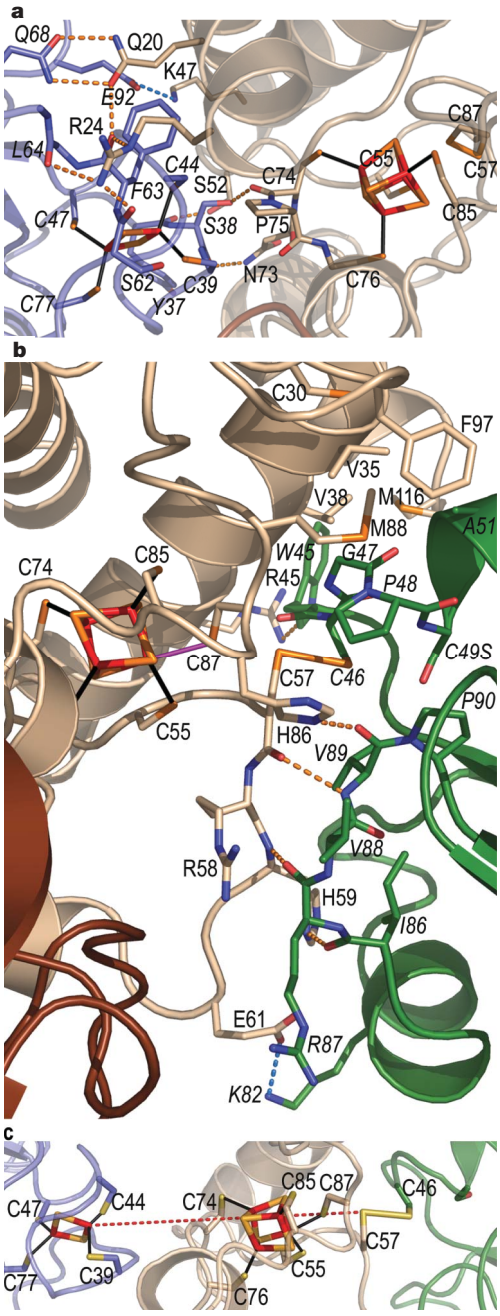

Figure 2 | Interactions of Fdx–FTR, FTR–Trx-*f*(C49S) and Fdx–FTR–Trx-*f*(C49S) complexes. a, **b**, Interactions between the catalytic subunit of FTR and **a**, Fdx and **b**, Trx-*f*(C49S). A disulphide bridge between Cys 57 of FTR and Cys 46 of Trx-*f*, forming the reaction intermediate, links the active sites of FTR and Trx. **c**, The close-up view of the active sites of the Fdx–FTR–Trx-*f*(C49S) complex. Electron transfer from the [2Fe–2S] cluster of Fdx to the intermolecular disulphide bond between the catalytic subunit of FTR and Trx-*f*(C49S) by way of the [4Fe–4S] cluster of FTR is represented as a red broken line. Hydrogen bonds and salt bridges are represented as orange and blue broken lines, respectively. Labels for amino acids in FTR are shown upright, and those for Fdx and Trx are shown in italics.

Although several positively charged residues in FTR and several negatively charged residues of Fdx were expected to be involved in the Fdx–FTR interaction[11], only one such interaction occurs: between FTR Lys 47 and Fdx Glu 92 (Fig. 2a). The charged surfaces thus serve mainly as general attractants rather than providing specificity. The variable subunit of FTR is not involved in the interaction; however, it may act as an additional attractant to facilitate the binding of Fdx to FTR. On the Fdx-binding side of the variable subunit there is a negatively charged patch that is complementary to a positively charged patch of Fdx. In photosynthetic cells, Fdx provides reducing equivalents to Fdx-$NADP^+$-reductase (FNR) to produce NADPH[12]. Interestingly, Fdx binds FTR and FNR in totally different manners (Supplementary Fig. 3).

After Fdx has delivered its electron to FTR, formation of the FTR intermediate **2** (which has been reduced by the addition of one electron, that is, 'one-electron-reduced') in the reaction cycle results from a direct transfer of the first electron through the unique iron of the cluster to the sulphur atom of Cys 87. Together with another electron, provided by the unique iron, the cluster is formally oxidized to the +3 oxidation state and the disulphide is cleaved[11,13]. Further insights into the mode of action of FTR have come from the *N*-ethylmaleimide modified enzyme (NEM-FTR). This chemically modified enzyme, in which the accessible active-site Cys has been alkylated, represents a stabilized form of a one-electron-reduced reaction intermediate (similar to species **2** in Fig. 3)[14]. The electron density map of this one-electron-reduced intermediate unambiguously shows that Cys 87 is coordinated to the unique iron atom (Fig. 4c), different from FTR at resting state, where Cys 87 is in van der Waals contact with the iron (species **1**) (Fig. 4a). This is in agreement with spectroscopic studies that demonstrated that the redox cycle of FTR involves interactions of the $[4Fe–4S]^{3+}$ cluster by means of a fifth cysteinate, probably on the unique iron[13,15]. Multi-coordinated geometry for a unique iron of a [4Fe–4S] cluster has been observed in proteins such as aconitase and radical *S*-adenosylmethionine proteins, in which they are coordinated by either oxygen or nitrogen[16–20]. However, penta-coordination involving two cysteine ligands at a unique iron site, as in the NEM-FTR cluster, has not been observed before.

The involvement of the cluster in forming an intermediate gives it a role beyond a simple electron transfer from the [4Fe–4S] cluster to the active-site disulphide. The $[4Fe–4S]^{2+/1+}$ and $[4Fe–4S]^{2+/3+}$ redox couples of FTR differ substantially from those of Fdx and Trx (refs 21, 22). However, by forming a five-coordinated intermediate, the redox potential of the $[4Fe–4S]^{2+/3+}$ couple of NEM-FTR is lowered from +420 mV to –210 mV, close to the redox potential of the Trx active-site disulphide.

The unique catalytic iron of one-electron-reduced FTR adopts distorted trigonal bipyramidal geometry. The distance between Cys 87 and the unique iron of the centre is reduced from 3.1 Å in the oxidized FTR to 2.6 Å as it becomes a thiolate ligand to the iron ion[23]. This long iron–sulphur bond has a lower energy than a normal bond of this type, which explains why it is readily cleaved when the one-electron-reduced FTR accepts an electron from Fdx. The Cys–iron distances, which influence the redox potential in different complexes, are given in Supplementary Table 2.

In the one-electron-reduced FTR (species **2**), the disulphide bridge is broken and the side chain of the more exposed active-site cysteine, Cys 57, is suited for a nucleophilic attack on the disulphide of Trx, forming a transient intermolecular disulphide bond (species **3**). Two types of Trx (Trx-*f* and Trx-*m*, which have different target enzyme specificities and different phylogenetic origins) in chloroplasts of higher plants use the same redox chemistry to regulate different target enzymes[24]. As predicted, a covalent bond is formed in the complex structures between the exposed Cys of Trx (Cys 46 and Cys 37 of Trx-*f* and Trx-*m*, respectively) and Cys57 of the catalytic subunit of FTR on the side opposite to the Fdx-binding site (Fig. 1b and Supplementary Fig. 4a). The use of Trx-mutants (Trx-*f*(C49S)

and Trx-*m*(C40S)) prevents scission of this intermolecular disulphide bond by the second Cys of the Trx active site.

The FTR–Trx complexes, which represent one-electron-reduced reaction intermediates containing an oxidized cluster in the +3 oxidation state (**3**), are stabilized by a number of interactions in addition to the intermolecular disulphide. The main interactions (Fig. 2b and Supplementary Fig. 4b) are between residues 82 to 90 of Trx-*f* (73 to 81 of Trx-*m*) and residues 57 to 61 of the catalytic subunit of FTR. These are completely conserved among FTRs, suggesting their crucial role in the function of FTR. Only local conformational changes occur on complex formation. The largest differences are caused by changes in the side-chain conformations at the Trx interaction face, which may contribute to the different specificities for Trx-*f* and Trx-*m*. Like Fdxs, the Trxs interact exclusively with the catalytic subunit of FTR. The interaction of Trx-*f* with FTR is similar to that of Trx-*m*, and the conformational difference between the complexes is a small rotation of the Trx molecule perpendicular to the flat FTR molecule (Supplementary Fig. 5).

The conserved Trp in the WCGPC motif of the Trxs provides a flat surface for interaction with its partners, mainly with hydrophobic residues[6]. In these complexes, Trx-*f* Trp 45 and Trx-*m* Trp 36 are not positioned to cover the surface of the Trx molecule in the common Trx conformation, but are instead flipped out, making interactions with FTR (Fig. 2b and Supplementary Fig. 4b). The interactions we observe differ substantially from those between the flavoenzyme Trx-reductase and Trx (Supplementary Fig. 6). The FTR–Trx complexes also demonstrate the presence of a five-coordinate iron atom similar to that in NEM-FTR (Figs 2b, 4d and Supplementary Fig. 4b). This confirmed that the one-electron-reduced FTR indeed is a reaction intermediate in which the disulphide bond has been cleaved and the exposed reactive FTR Cys 57 has been freed to react with Trx.

FTR–Trx complexes can be efficiently reduced by Fdxs. This requires the formation of a transient Fdx–FTR–Trx complex (**3**→**5** in Fig. 3). Experimental evidence for such complexes has been obtained by chromatography and difference spectroscopy[25]. The crystal structure of this ternary complex shows that FTR accommodates Fdx and Trx-*f* simultaneously without major conformational changes (Fig. 1c, 2c and Supplementary Fig. 9) because the overall structure of the Fdx–FTR–Trx-*f* complex is similar to those of the FTR–Trx-*f*, FTR–Trx-*m* and Fdx–FTR complexes (Supplementary Fig. 7). However, the molecules are rotated in relation to each other, similar to the different position of Trx-*f* and Trx-*m* in relation to FTR (Supplementary Fig. 5). There is an extra salt bridge interaction between FTR Glu 61 and Trx-*f* Arg 87 in this ternary complex, which is absent in FTR–Trx-*f* complex. The buried surface area between Fdx and FTR increases from 430 Å^2 in the Fdx–FTR complex to 680 Å^2 in the ternary complex, whereas the interface area between FTR and Trx-*f* increases from 650 Å^2 in the FTR–Trx-*f* complex to 830 Å^2, indicating that the ternary complex is more stable.

The unusually thin FTR is ideal for electron transfer and for allowing fast access for the delivery of electrons from Fdx to the disulphide on the other side of the molecule. The shortest distance between the iron centre of Fdx and a cysteine of Trx is approximately 20 Å. The [2Fe–2S], [4Fe–4S] and redox-active disulphide bonds of both FTR

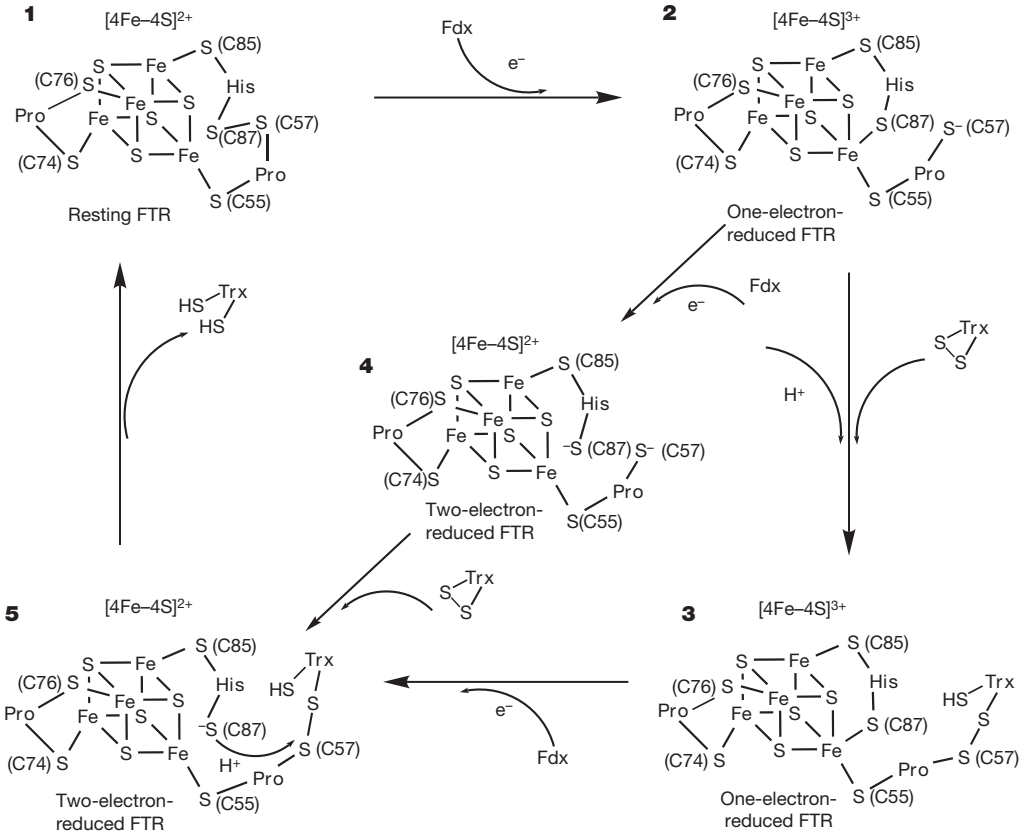

Figure 3 | FTR mechanism proposed on the basis of current structural and spectroscopic[15] investigations. One electron from Fdx, together with one electron from the iron–sulphur cluster, is used to cleave the disulphide bridge of FTR. Cys 87 is stabilized by forming the fifth ligand to the cluster, and Cys 57 is free to attack the disulphide bond of Trx. The cluster of this species **2** shows +3 oxidation state. After thiol–disulphide interchange between Cys 57 of FTR and Trx, the disulphide bond of Trx is cleaved and a FTR–Trx complex with a mixed disulphide bond is formed as species **3**. The second electron can be delivered by a new Fdx either to the one-electron-reduced FTR or to the FTR–Trx complex. Here, the two-electron-reduced species **4** can form and the reaction pathway splits. In both cases, Fdx reduces the iron–sulphur cluster back to its original +2 oxidation state and Cys 87 is freed. Then Cys 87 attacks the heterodisulphide bridge of FTR–Trx complex (short-lived species **5**), releasing the fully reduced thioredoxin, and the FTR active-site disulphide bond reforms (species **1**). The two-electron-reduced FTR species **4**, with two free thiols, can instantly reduce and release the reduced Trx.

and Trx are aligned in a straight line—an alignment that should maximize the electron-transfer rate (Fig. 2c). Here the complex structure suggests an electron transfer pathway from a [2Fe–2S] cluster to the substrate disulphide bridge that involves several reactions: electron transfer from [2Fe–2S] to [4Fe–4S] clusters, cleavage of a disulphide bond by the [4Fe–4S] centre, and dithiol–disulphide interchange.

Before its interaction with Trx, the one-electron-reduced FTR intermediate can accept a second electron and yield a two-electron-reduced species (**4** in Fig. 3); this may lead to an alternative reaction pathway, as suggested in recent spectroscopic studies[15]. In the structure of two-electron-reduced FTR, the disulphide bridge is broken, FTR Cys 87 is detached from the unique iron, and the substrate-interacting FTR Cys 57 is exposed and hydrogen-bonded to a water molecule (Fig. 4b). FTR His 86 rotates towards the cluster and interacts with sulphur atoms of the $[4Fe–4S]^{2+}$ cluster and with FTR Cys 55 (Supplementary Fig. 8). The hydrogen-bonding interactions involving His 86 and Cys 55 or the proximity of the positively charged His 86 to the cluster may be responsible for the anomalous electronic properties of the $[4Fe–4S]^{2+}$ cluster[15,26]. The proximity of His 86 to the iron–sulphur centre can also increase the redox potential of FTR[27], facilitating the reduction of the one-electron-reduced intermediates.

Because one-electron-reduced (species **2**) and two-electron-reduced (species **4**) FTR should both be able to cleave the disulphide bridge with the reactive Cys 57 and form the intermolecular heterodisulphide bond intermediate, the FTR reduction efficiency may be increased. The two-electron-reduced species can interact with oxidized Trx and form a FTR–Trx complex (species **5**) in a mechanism analogous to the one-electron-reduced intermediate. However, this complex should be rather short-lived, because the freed Cys 87 thiol is close to Cys 57 and ready to attack and cleave the heterodisulphide to complete the reduction of Trx and restore the active-site disulphide of FTR. Under normal conditions, the one-electron pathway should be preferred, but, under over-reducing conditions, which occur when there is not enough electron acceptor (for example, CO_2), the two-electron pathway could become more important.

We have captured FTR in all stable redox states in a catalytic cycle. The results illustrate how a disulphide bridge can be cleaved with reducing power donated by an iron–sulphur centre. Our structural analysis shows that only the substrate-exposed unique iron of the cluster performs the chemistry and that coordination variation plays a pivotal role in the catalytic function of the cluster. These results provide key insights into the important site-specific chemistry of the iron–sulphur cluster and reveal its novel mode of action. They may also have implications for the mechanisms of related [4Fe–4S]-containing proteins, such as the radical *S*-adenosylmethionine enzymes and heterodisulphide reductases[26,28,29].

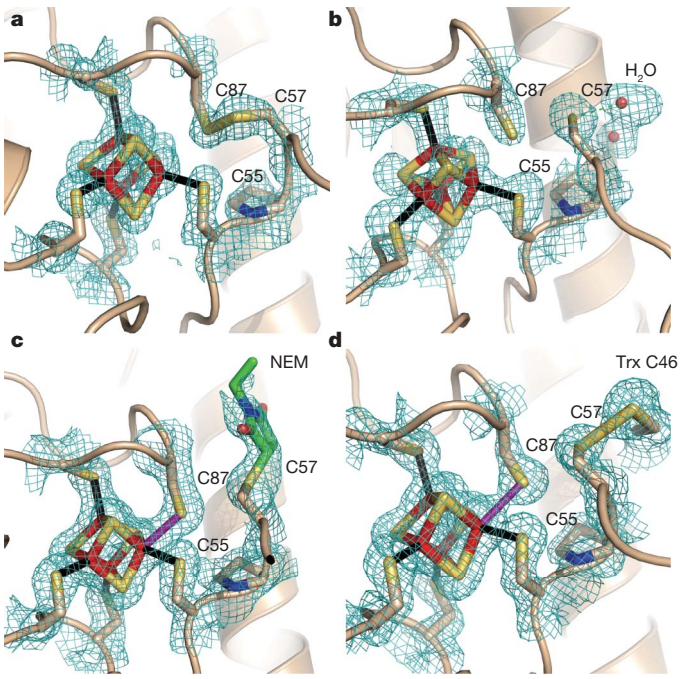

Figure 4 | Comparison of the active sites of FTR at different reaction states. Simulated annealing $2F_o–F_c$ omit electron maps, in which FTR Cys 55, Cys 57, Cys 87 and the [4Fe–4S] cluster were omitted, contoured at 1σ around the active-site disulphide and [4Fe–4S] cluster of FTR. The [4Fe–4S] cluster of FTR is represented as sticks, in which iron and sulphur atoms are coloured red and orange, respectively. Water molecules are shown as red spheres. **a**, Resting enzyme[11]. **b**, Two-electron-reduced FTR. **c**, NEM-FTR. **d**, FTR–Trx-*f*(C49S) complex.

METHODS SUMMARY

Synechocystis FTR and Fdx, mutant spinach Trx-*f* and Trx-*m* were overexpressed in *Escherichia coli*. NEM-FTR was obtained following the method described earlier[30]. Two-electron-reduced FTR was obtained by reducing the crystals of oxidized FTR (ref. 11) with 100 mM dithionite in presence of 50–100 mM methyl viologen for 2 h using gradient soaking in anaerobic conditions. The non-covalent Fdx–FTR complex was obtained by mixing the two proteins at equimolar concentrations and incubating overnight at 4 °C. Covalent FTR−Trx complexes were obtained by mixing wild-type FTR with an equimolar amount of Trx-mutant. The mixture was reduced with 10 mM dithiothreitol (DTT), diafiltered with the same buffer without DTT and left overnight at 4 °C under aerobic conditions. Fdx–FTR–Trx-*f* complex was obtained by mixing Fdx and the FTR–Trx-*f* complex at equimolar concentrations. All proteins were crystallized by hanging- or sitting-drop vapour diffusion methods. X-ray diffraction data were collected under liquid-nitrogen cryoconditions at 100 K. Data were processed with the HKL2000 or HKL suite of programs (HKL Research). The crystal structures were determined by the molecular replacement method. Oxidized FTR was used as the search model for NEM−FTR and reduced FTR. Oxidized FTR, Trx or Fdx were used for the molecular replacement calculation of the complexes.

Full Methods and any associated references are available in the online version of the paper at www.nature.com/nature.

1. Buchanan, B. B. & Balmer, Y. Redox regulation: a broadening horizon. *Annu. Rev. Plant Biol.* **56,** 187–220 (2005).
2. Schürmann, P. Redox signaling in the chloroplast: the ferredoxin/thioredoxin system. *Antioxid. Redox Signal.* **5,** 69–78 (2003).
3. Johnson, D. C., Dean, D. R., Smith, A. D. & Johnson, M. K. Structure, function, and formation of biological iron–sulfur clusters. *Annu. Rev. Biochem.* **74,** 247–281 (2005).
4. Kurisu, G. *et al.* Structure of the electron transfer complex between ferredoxin and ferredoxin-$NADP^+$ reductase. *Nature Struct. Biol.* **8,** 117–121 (2001).
5. Morales, R. *et al.* A redox-dependent interaction between two electron-transfer partners involved in photosynthesis. *EMBO Rep.* **1,** 271–276 (2000).
6. Lennon, B. W., Williams, C. H. Jr & Ludwig, M. L. Twists in catalysis: alternating conformations of *Escherichia coli* thioredoxin reductase. *Science* **289,** 1190–1194 (2000).
7. Dai, S. *et al.* How does light regulate chloroplast enzymes? Structure–function studies of the ferredoxin/thioredoxin system. *Q. Rev. Biophys.* **33,** 67–108 (2000).
8. van den Heuvel, R. H. *et al.* The active conformation of glutamate synthase and its binding to ferredoxin. *J. Mol. Biol.* **330,** 113–128 (2003).
9. Xu, X. *et al.* Ferredoxin/ferredoxin–thioredoxin reductase complex: complete NMR mapping of the interaction site on ferredoxin by gallium substitution. *FEBS Lett.* **580,** 6714–6720 (2006).
10. Onuchic, J. N., Beratan, D. N., Winkler, J. R. & Gray, H. B. Pathway analysis of protein electron-transfer reactions. *Annu. Rev. Biophys. Biomol. Struct.* **21,** 349–377 (1992).
11. Dai, S., Schwendtmayer, C., Schürmann, P., Ramaswamy, S. & Eklund, H. Redox signaling in chloroplasts: cleavage of disulfides by an iron–sulfur cluster. *Science* **287,** 655–658 (2000).
12. Knaff, D. B. in *Advances in Photosynthesis* (eds Ort, D. R. & Yocum, C. F.) 333–361 (Kluwer Academic, Dordrecht, 1996).
13. Jameson, G. N. *et al.* Spectroscopic evidence for site specific chemistry at a unique iron site of the [4Fe–4S] cluster in ferredoxin:thioredoxin reductase. *J. Am. Chem. Soc.* **125,** 1146–1147 (2003).
14. Staples, C. R. *et al.* Role of the $[Fe_4S_4]$ cluster in mediating disulfide reduction in spinach ferredoxin:thioredoxin reductase. *Biochemistry* **37,** 4612–4620 (1998).

15. Walters, E. M. *et al.* Spectroscopic characterization of site-specific [Fe_4S_4] cluster chemistry in ferredoxin:thioredoxin reductase: implications for the catalytic mechanism. *J. Am. Chem. Soc.* **127,** 9612–9624 (2005).
16. Berkovitch, F., Nicolet, Y., Wan, J. T., Jarrett, J. T. & Drennan, C. L. Crystal structure of biotin synthase, an *S*-adenosylmethionine-dependent radical enzyme. *Science* **303,** 76–79 (2004).
17. Hanzelmann, P. & Schindelin, H. Crystal structure of the *S*-adenosylmethionine-dependent enzyme MoaA and its implications for molybdenum cofactor deficiency in humans. *Proc. Natl Acad. Sci. USA* **101,** 12870–12875 (2004).
18. Lauble, H., Kennedy, M. C., Beinert, H. & Stout, C. D. Crystal structures of aconitase with trans-aconitate and nitrocitrate bound. *J. Mol. Biol.* **237,** 437–451 (1994).
19. Layer, G., Moser, J., Heinz, D. W., Jahn, D. & Schubert, W. D. Crystal structure of coproporphyrinogen III oxidase reveals cofactor geometry of Radical SAM enzymes. *EMBO J.* **22,** 6214–6224 (2003).
20. Lepore, B. W., Ruzicka, F. J., Frey, P. A. & Ringe, D. The X-ray crystal structure of lysine-2,3-aminomutase from *Clostridium subterminale. Proc. Natl Acad. Sci. USA* **102,** 13819–13824 (2005).
21. Staples, C. R. *et al.* The function and properties of the iron–sulfur center in spinach ferredoxin:thioredoxin reductase: a new biological role for iron–sulfur clusters. *Biochemistry* **35,** 11425–11434 (1996).
22. Hirasawa, M. *et al.* Oxidation–reduction properties of chloroplast thioredoxins, ferredoxin:thioredoxin reductase, and thioredoxin *f*-regulated enzymes. *Biochemistry* **38,** 5200–5205 (1999).
23. Giastas, P. *et al.* The structure of the 2[4Fe–4S] ferredoxin from *Pseudomonas aeruginosa* at 1.32-Å resolution: comparison with other high-resolution structures of ferredoxins and contributing structural features to reduction potential values. *J. Biol. Inorg. Chem.* **11,** 445–458 (2006).
24. Buchanan, B. B., Schürmann, P., Decottignies, P. & Lozano, R. M. Thioredoxin: a multifunctional regulatory protein with a bright future in technology and medicine. *Arch. Biochem. Biophys.* **314,** 257–260 (1994).
25. Glauser, D. A., Bourquin, F., Manieri, W. & Schürmann, P. Characterization of ferredoxin:thioredoxin reductase modified by site-directed mutagenesis. *J. Biol. Chem.* **279,** 16662–16669 (2004).
26. Walters, E. M. & Johnson, M. K. Ferredoxin:thioredoxin reductase: disulfide reduction catalyzed via novel site-specific [4Fe–4S] cluster chemistry. *Photosynth. Res.* **79,** 249–264 (2004).
27. Chen, K. *et al.* Crystal structures of ferredoxin variants exhibiting large changes in [Fe–S] reduction potential. *Nature Struct. Biol.* **9,** 188–192 (2002).
28. Duin, E. C., Madadi-Kahkesh, S., Hedderich, R., Clay, M. D. & Johnson, M. K. Heterodisulfide reductase from *Methanothermobacter marburgensis* contains an active-site [4Fe–4S] cluster that is directly involved in mediating heterodisulfide reduction. *FEBS Lett.* **512,** 263–268 (2002).
29. Chen, D., Walsby, C., Hoffman, B. M. & Frey, P. A. Coordination and mechanism of reversible cleavage of *S*-adenosylmethionine by the [4Fe–4S] center in lysine 2,3-aminomutase. *J. Am. Chem. Soc.* **125,** 11788–11789 (2003).
30. Schürmann, P. & Gardet-Salvi, L. Chemical modification of the active site of ferredoxin–thioredoxin reductase. *Chimia* **47,** 245–246 (1993).

Acknowledgements We thank J. Kappler, P. Marrack and J. Bolin for support and encouragement; the Zuckerman/Canyon Ranch and A. Lapporte for support of the X-ray and computing facilities; the Howard Hughes Medical Institute beamlines at Advanced Light Source (ALS), the Structural Biology Centre at Advanced Photon Source (APS), and the European Synchrotron Radiation Facility (ESRF) for synchrotron data. H.E. was supported by the Swedish Council for Forestry and Agricultural Research and the Swedish Natural Science Research Council, and P.S. was supported by the Schweizerischer Nationalfonds.

Author Contributions S.D., R.F., D.A.G., F.B., W.M. and P.S. performed the experiments. S.D., R.F., P.S. and H.E. designed and prepared the manuscript.

METHODS

Sample preparation and crystallization. *Synechocystis* FTR shows no functional difference from spinach FTR, but is significantly more stable[31]. FTR and Fdx from *Synechocystis* sp. PCC6803 and mutant spinach Trx-*f*(C49S) were expressed and purified, as previously described[25,32]. Mutant spinach Trx-*m*(C40S) is based on the recombinant Trx-*m* described earlier[33], from which the amino-terminal extra peptide of six residues was removed to obtain a protein corresponding in its size exactly to spinach Trx-m_c[34]. The mutant construct was cloned into the expression plasmid pET-3c and expressed in *E. coli* strain BL21(DE3).

NEM-FTR was obtained following the method described in detail earlier[30]. FTR was reduced in the light with thylakoids and Fdx under argon using thylakoids capable of only photosystem I (in which there is no oxygen evolution), with ascorbate/dichloro-phenolindophenol as the electron donor system instead of water. After five minutes in the light, NEM (Fluka) was added, and incubation continued for two minutes. Excess NEM was quenched by addition of 2-mercaptoethanol as the light was turned off. The mixture was centrifuged, desalted on G-25 column, and the NEM-FTR separated from Fdx and contaminating proteins from the thylakoids by ion exchange chromatography[30]. NEM-FTR was crystallized at room temperature by hanging-drop vapour diffusion against 1 ml mother liquor containing 2.1 M ammonium sulphate and 100 mM sodium acetate, pH 5.4. In all crystallization setups, 2.0 µl of protein solution (16 mg ml^{-1}, in 20 mM triethanolamine (TEA)-Cl buffer, pH 7.5) was mixed with an equal volume of reservoir solution.

Crystals of oxidized FTR were grown at room temperature by the sitting-drop vapour diffusion method. Each drop, consisting of 2 µl protein solution and an equal volume of reservoir solution, was equilibrated against 1 ml reservoir solution containing 1.8 M ammonium sulphate and 100 mM sodium acetate buffer around pH 5.2 (ref. 11). The sample was concentrated to 24 mg ml^{-1} in 50 mM Tris-Cl buffer pH 7.5. The crystals were usually obtained with the help of micro-seeding technique[35]. All crystallization trials were performed in an anaerobic chamber with an O_2 level of less than 5 parts per million. The solutions were degassed thoroughly before moving into the glove box. Two-electron-reduced FTR was obtained by reducing the crystals of oxidized FTR with 100 mM dithionite in presence of 50–100 mM methyl viologen[36] for two hours using gradient soaking.

The noncovalent Fdx–FTR complex was obtained by mixing the two proteins at equimolar concentrations and incubating overnight at 4 °C under conditions that were shown to allow complex formation[25]. Crystallization was performed by the hanging- or sitting-drop vapour diffusion method. In all the experiments, 1.5–2 µl protein solution and 1.5–2 µl precipitant solution were equilibrated against 1 ml precipitant solution. Fdx–FTR complex (27 mg ml^{-1}, in 50 mM Tris-Cl buffer, pH 7.5) crystallized at 20 °C in 32% polyethylene glycol (PEG)8000 and 0.1 M cacodylate, pH 5.5. Crystals normally formed within one week.

Mutation of the buried active-site Cys residue of Trx allows one to stabilize the transient intermolecular disulphide bridge, a method that has been used extensively in several studies[6,37]. Using this approach, we generated covalent complexes between FTR and mutant Trx-*m*(C40S) and Trx-*f*(C49S). Covalent FTR−Trx complexes were obtained by mixing concentrated wild-type FTR with an equimolar amount of Trx mutant. The mixture in 20 mM TEA-Cl buffer, pH 7.3, was reduced with 10 mM DTT, diafiltered with the same buffer without DTT, and left overnight at 4 °C with very slow stirring to allow oxygen to function as electron acceptor. The FTR–Trx complexes formed were re-purified by ion exchange chromatography to remove unreacted proteins from the complex[25]. Crystallization experiments were carried out by the hanging-drop vapour diffusion method. In a typical trial, 2 µl protein samples were mixed with an equal amount of mother liquor and then equilibrated against 1 ml reservoir solution. Crystals of FTR–Trx-*f* (18 mg ml^{-1}) were obtained within two weeks in 1.8–2.0 M ammonium sulphate, 0.1 M KNa tartrate and 0.2 M sodium citrate, pH 5.2–6.0, at 20 °C. Crystals of FTR–Trx-*m* complex (20 mg ml^{-1}) were grown at 15 °C in 20% (w/v) PEG3350, 0.2 M sodium fluoride and 0.1 M HEPES-OH, pH 6.0. Crystals were obtained within three months.

Fdx–FTR–Trx-*f* complex was obtained by incubating at 4 °C overnight after mixing equimolar concentrations of Fdx and FTR–Trx-*f*. Subsequently, the complex was purified with a size-exclusion column, Superdex 75 (GE Healthcare), at 4 °C. Crystallization trials were performed by the vapour-diffusion technique using the hanging-drop method. Optimized crystals were obtained at 20 °C in hanging drops by mixing 1 µl of 30 mg ml^{-1} protein in 20 mM TEA-Cl buffer, pH 7.5, and 1 µl reservoir solution containing 2.0 M ammonium sulphate, 0.1 M KNa tartrate and 0.2 M sodium citrate, pH 5.6.

Structure determination. All X-ray diffraction data were collected under liquid nitrogen cryo-conditions at 100 K. Before refinement, an independent set of 5% reflections was set aside for the free R (R_{free}) value calculation for all data sets. No sigma cutoffs were used in all refinements. Both conventional R-factor (R_{cryst}) and R_{free} (ref. 38) were used to monitor the progress of refinement. The models were subjected to several rounds of alternating simulated annealing/positional refinement in CNS[39] followed by B-factor refinement in CNS or REFMAC[40]. Model building was performed using the program O[41]. Several residues of the amino termini and carboxy termini of both the catalytic subunit and the variable subunit of FTR are disordered in all structures; however, the majority of the residues are well defined except several solvent-exposed side chains. Simulated annealing omit maps were routinely used to remove the model bias. The CNS parameter and topology files of [4Fe–4S] and [2Fe–2S] clusters were generated by Hetero-compound Information Centre — Uppsala (HIC-Up)[42]. The distance between Cys 87 Sγ and Fe was not restrained. However, the distances between Sγ of the cluster-ligating cysteines and iron were restrained to 2.3 Å in initial refinements. After R_{free} dropped below 30%, the bond restraints between Cys Sγ and iron were lifted in refinements. All models have good stereochemistry, as determined by the program PROCHECK[43]. Data collection and refinement statistics including Ramachandran plot statistics are summarized in Supplementary Table 1. Surface areas were calculated with GRASP[44]. Figures were prepared using PyMOL[45].

The Fdx–FTR complex crystals were flash-cooled in liquid nitrogen after a 10–30 s soak in a cryoprotection solution consisting of the reservoir solution with an addition of 27% (w/v) PEG4000. X-ray data were measured at SBC beamline ID-19 at the APS of Argonne National Laboratory. The data were indexed, integrated, scaled and merged using HKL2000 (ref. 46). The structure of Fdx–FTR was determined by molecular replacement using the program AMoRe[47] by using *Synechocystis* Fdx (Protein Data Bank code 1DOX, ref. 48) and *Synechocystis* oxidized FTR (Protein Data Bank code 1DJ7, ref. 11) as search models.

FTR–Trx-*f* crystals were flash-frozen in a cryoprotection solution consisting of the reservoir solution with addition of 25% (v/v) glycerol in liquid nitrogen. Diffraction data were collected on a Rigaku R2U rotating anode using a MSC RaxisIV image plate detector. The four data sets collected on four crystals were indexed, integrated, scaled and merged using HKL2000 (ref. 46). The structure was determined by the molecular replacement program AMoRe[47] using the structure of *Synechocystis* FTR[11] as a search model. After an initial round of refinement, Trx-*f* could be manually modelled into the $2F_o–F_c$ map using O[41].

FTR–Trx-*m* crystals were flash-cooled in liquid nitrogen without addition of cryoprotectant. Diffraction data were collected on beamline ID14-4 at the ESRF, using an ADSC detector. The data were integrated using MOSFLM[49] and scaled using SCALA[50]. The structure was solved with the molecular replacement program MOLREP[51], using the FTR–Trx-*f* complex as a search model. The FTR–Trx-*m* crystals have two complex molecules in the asymmetric unit, and the electron density is well defined for both FTR–Trx-*m* molecules.

NEM-FTR and two-electron-reduced FTR crystals were flash-frozen in liquid nitrogen after a soak lasting 2–10 s in mother liquor solutions containing 20% glycerol. X-ray data of two-electron-reduced FTR were measured at SBC beamline ID-19 at the APS. The data were indexed and integrated using DENZO and reduced using SCALEPACK[46]. The first model of reduced FTR was obtained by rigid body refinement in REFMAC[40] in CCP4 using the structure of the oxidized FTR[11] as a model. There was a huge negative density (more than 5σ) at the active-site disulphide bond in the different Fourier maps, and a small positive at 3σ on surface of the protein, in agreement with the breakage of the disulphide bond. Data sets of NEM-FTR were collected on beamline 8.2.1 at ALS of the Lawrence Berkeley National Laboratory. Data were processed and scaled with HKL2000 (ref. 46). Molecular replacement was performed using the program AMoRe[47], and the oxidized FTR structure[11] without the iron–sulphur cluster was used as a search model. One single high peak was obtained after rotation and translation functions. In the initial maps, we could clearly see the iron–sulphur cluster and there was an extra positive density extended from the density of Cys 57. NEM could be nicely modelled into this positive density. Phase improvement and refinement of both structures were performed by CNS[39], and model was manually adjusted using the program O[41].

Fdx–FTR–Trx-*f* crystals were flash-frozen in a cryoprotection solution consisting of the reservoir solution with addition of 20% (v/v) glycerol in liquid nitrogen. X-ray diffraction data were collected at beamline 8.2.1 at ALS using a CCD detector. The data were indexed, integrated, scaled and merged using HKL2000 (ref. 46). The structure was determined by the molecular replacement program AMoRe[47] using the structures of FTR–Trx-*f* and *Synechocystis* Fdx as search models. The solution was unambiguous and showed presence of one complex within the asymmetric unit.

31. Manieri, W. *et al.* N-terminal truncation of the variable subunit stabilizes spinach ferredoxin:thioredoxin reductase. *FEBS Lett.* **549**, 167–170 (2003).
32. Balmer, Y. & Schürmann, P. Heterodimer formation between thioredoxin *f* and fructose 1,6-bisphosphatase from spinach chloroplasts. *FEBS Lett.* **492**, 58–61 (2001).

33. Schürmann, P. Ferredoxin:thioredoxin system. *Methods Enzymol.* **252,** 274–283 (1995).
34. Wedel, N., Clausmeyer, S., Herrmann, R. G., Gardet-Salvi, L. & Schürmann, P. Nucleotide sequence of cDNAs encoding the entire precursor polypeptide for thioredoxin *m* from spinach chloroplasts. *Plant Mol. Biol.* **18,** 527–533 (1992).
35. Stura, E. A. in *Crystallization of Nucleic Acids and Proteins. A Practical Approach* (eds Ducruix, A. & Giegé, R.) 99–126 (Oxford Univ. Press, New York, 1999).
36. Schürmann, P., Stritt-Etter, A. L. & Li, J. Reduction of ferredoxin:thioredoxin reductase by artificial electron donors. *Photosynth. Res.* **46,** 309–312 (1995).
37. Balmer, Y. *et al.* Proteomics gives insight into the regulatory function of chloroplast thioredoxins. *Proc. Natl Acad. Sci. USA* **100,** 370–375 (2003).
38. Brunger, A. T. Free R value: a novel statistical quantity for assessing the accuracy of crystal structures. *Nature* **355,** 472–475 (1992).
39. Brunger, A. T. *et al.* Crystallography & NMR system: a new software suite for macromolecular structure determination. *Acta Crystallogr. D* **54,** 905–921 (1998).
40. Murshudov, G. N., Vagin, A. A. & Dodson, E. J. Refinement of macromolecular structures by the maximum-likelihood method. *Acta Crystallogr. D* **53,** 240–255 (1997).
41. Jones, T. A., Zou, J. Y., Cowan, S. W. & Kjeldgaard, M. Improved methods for building protein models in electron density maps and the location of errors in these models. *Acta Crystallogr. A* **47,** 110–119 (1991).
42. Kleywegt, G. J., Henrick, K., Dodson, E. J. & van Aalten, D. M. Pound-wise but penny-foolish: how well do micromolecules fare in macromolecular refinement? *Structure* **11,** 1051–1059 (2003).
43. Laskowski, R. A., MacArthur, M. W., Moss, D. S. & Thornton, J. M. PROCHECK: a program to check the stereochemical quality of protein structures. *J. Appl. Crystallogr.* **26,** 283–291 (1993).
44. Nicholls, A., Sharp, K. A. & Honig, B. Protein folding and association: insights from the interfacial and thermodynamic properties of hydrocarbons. *Proteins* **11,** 281–296 (1991).
45. DeLano, W. The PyMOL Molecular Graphics System. ⟨http://www.pymol.org⟩ (2002).
46. Otwinowski, Z. & Minor, W. Processing of X-ray diffraction data collected in oscillation mode. *Methods Enzymol.* **276,** 307–326 (1997).
47. Navaza, J. AMoRe: an automated package for molecular replacement. *Acta Crystallogr. A* **50,** 157–163 (1994).
48. Lelong, C., Setif, P., Bottin, H., Andre, F. & Neumann, J. M. ^{1}H and ^{15}N NMR sequential assignment, secondary structure, and tertiary fold of [2Fe–2S] ferredoxin from *Synechocystis* sp. PCC 6803. *Biochemistry* **34,** 14462–14473 (1995).
49. Powell, H. R. The Rossmann Fourier autoindexing algorithm in MOSFLM. *Acta Crystallogr. D* **55,** 1690–1695 (1999).
50. Collaborative Computational Project No 4. The *CCP4* suite: programs for protein crystallography. *Acta Crystallogr. D* **50,** 760–763 (1994).
51. Vagin, A. & Teplyakov, A. MOLREP: an automated program for molecular replacement. *J. Appl. Crystallogr.* **30,** 1022–1025 (1997).

Structural Snapshots along the Reaction Pathway of Ferredoxin:Thioredoxin Reductase

Shaodong Dai, Rosmarie Friemann, Dominique A. Glauser, Florence Bourquin, Wanda Manieri, Peter Schürmann and Hans Eklund

Supplementary Figure 1. Light activation/deactivation of chloroplast enzymes by the FTR system.

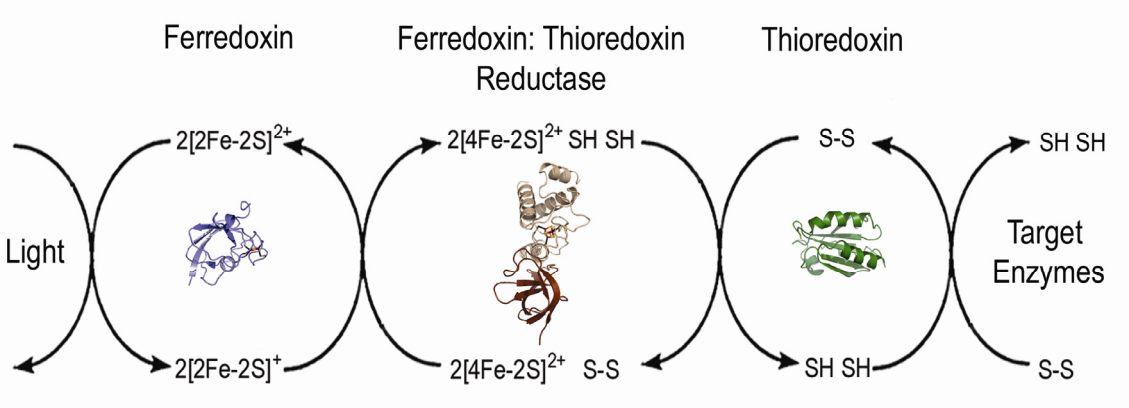

In light, photosystem I reduces ferredoxin which through FTR reduces thioredoxins that activate/deactivate target enzymes. This is the central redox signalling pathway that causes chloroplasts to respond to light and helps avoid futile cycling by the simultaneous functioning of assimilatory and dissimilatory reactions and appears also to be involved in plastid gene expression and detoxification of reactive oxygen species.

Supplementary Figure 2. Possible electron transfer pathways in the Fdx-FTR complex.

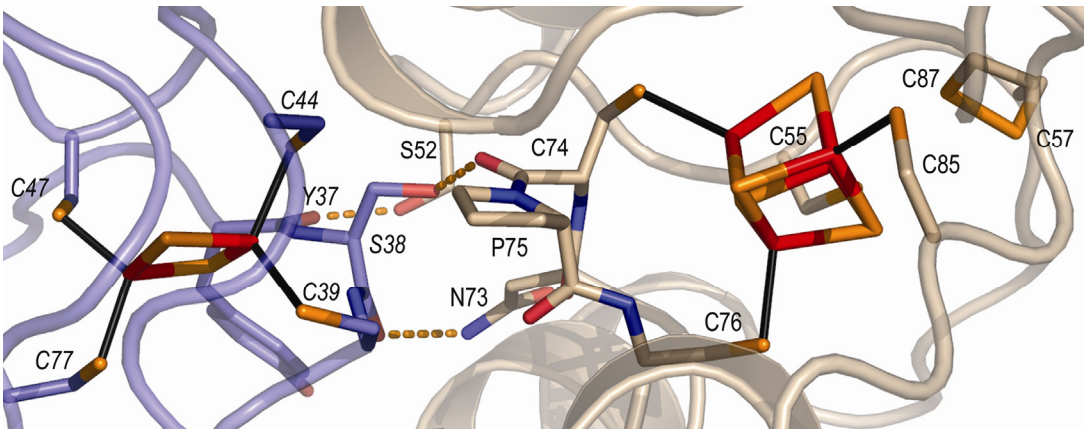

Possible routes of electron transfer (shown as orange dotted lines) from the Fdx [2Fe-2S] cluster to the [4Fe-4S] cluster of the catalytic subunit of FTR. The most probable pathway for electron transfer between the two clusters is through the side chain of Fdx Ser38 and the [4Fe-4S] cluster coordinating Cys74 main chain oxygen of the catalytic subunit of FTR. The carbonyl oxygen of Ser38 is furthermore hydrogen bonded to the side-chain of residue Asn73 of the catalytic subunit of FTR providing an alternative electron transfer route. A third possible path is through the carbonyl oxygen of Tyr37 of Fdx, which forms a hydrogen bond to the side chain of Ser52 of the catalytic subunit of FTR. Fdx and the catalytic subunit of FTR are coloured in blue and beige, respectively. The [2Fe-2S] cluster of Fdx and [4Fe-4S] cluster are represented in sticks, where the iron and sulphur atoms are coloured red and orange, respectively. Labels for FTR and Fdx amino acid residues are shown in regular and italics, respectively.

Supplementary Figure 3. Comparison of the interactions of the *Synechocystis* Fdx-FTR and maize Fdx-FNR complexes.

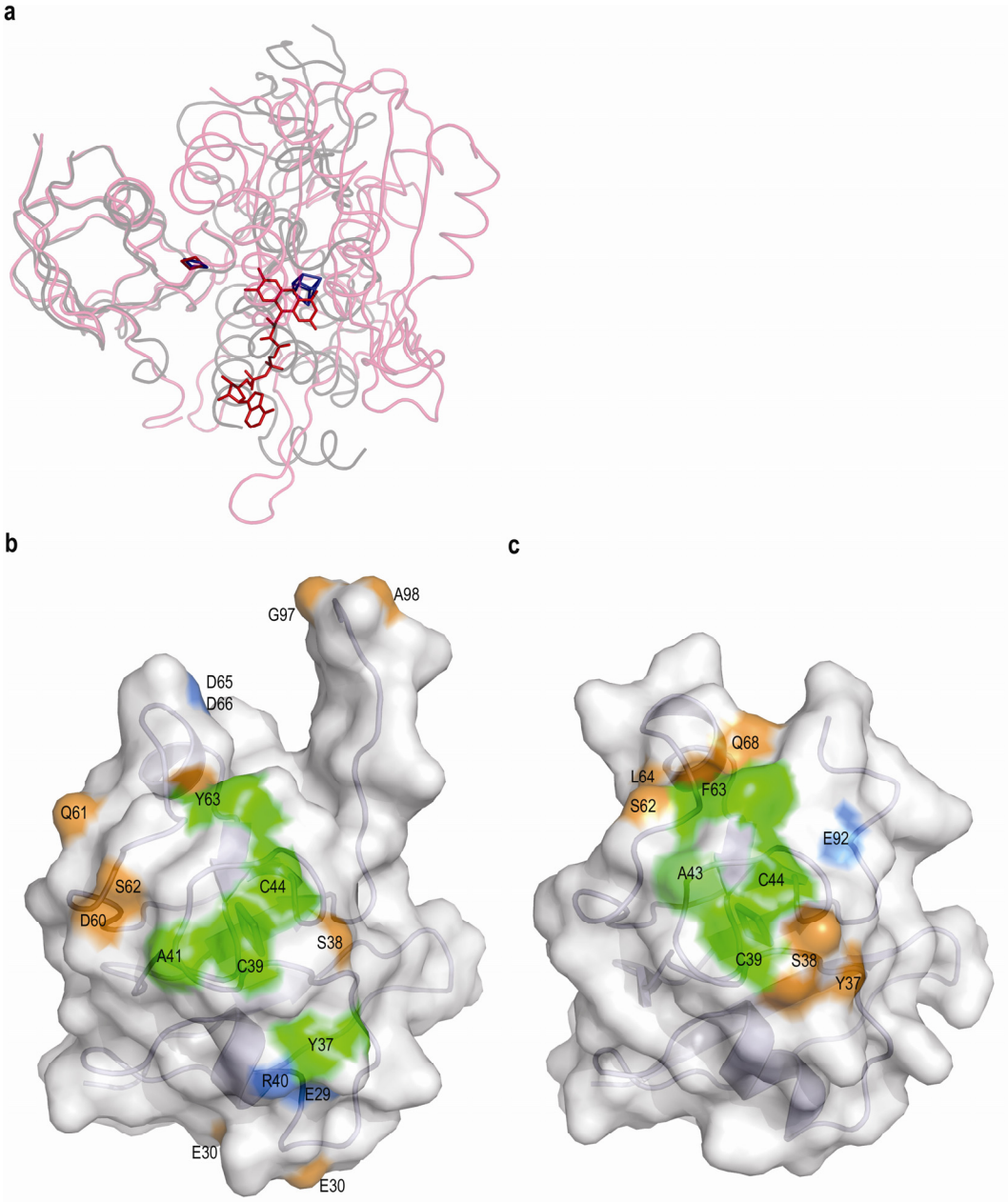

a) Superposition of Fdx-FNR (pink, pdb code: 1GAQ[1]) and Fdx-FTR (grey), where the Fdxs are aligned (left part of figure). Flavin adenine dinucleotide (FAD) of FNR (red) and the iron-sulphur clusters of FTR (blue) and Fdx (red and

blue) are shown in sticks. The interaction surface of the Fdx-FTR complex is around 430 $Å^2$, much smaller than that of Fdx-FNR.

b) Surface representation of the interaction area of Fdx in the Fdx-FNR complex where all atoms that are involved forming hydrogen bonds, salt bridges or hydrophobic interactions with FNR are coloured orange, blue and green, respectively.

c) Surface representation of the interaction area of Fdx in the Fdx-FTR complex. Colour coding as in b.

Several charged residues, including four intermolecular salt bridges are located on either side of the hydrophobic intermolecular contact area in the Fdx-FNR complex (b). In contrast, the only salt bridge in the Fdx-FTR complex (c) between Lys47 of the catalytic subunit of FTR and Fdx Glu92 has no counterpart in the Fdx-FNR complex. In the Fdx-FNR, Fdx Ser38, which is suggested to mediate the electron transfer in Fdx-FTR, forms a hydrogen bond to the residue preceding the FNR C-terminal Tyr314 that sandwiches against the isoalloxazine ring of the FAD.

Supplementary Figure 4. Crystal structures of FTR-Trx-*m* complex.

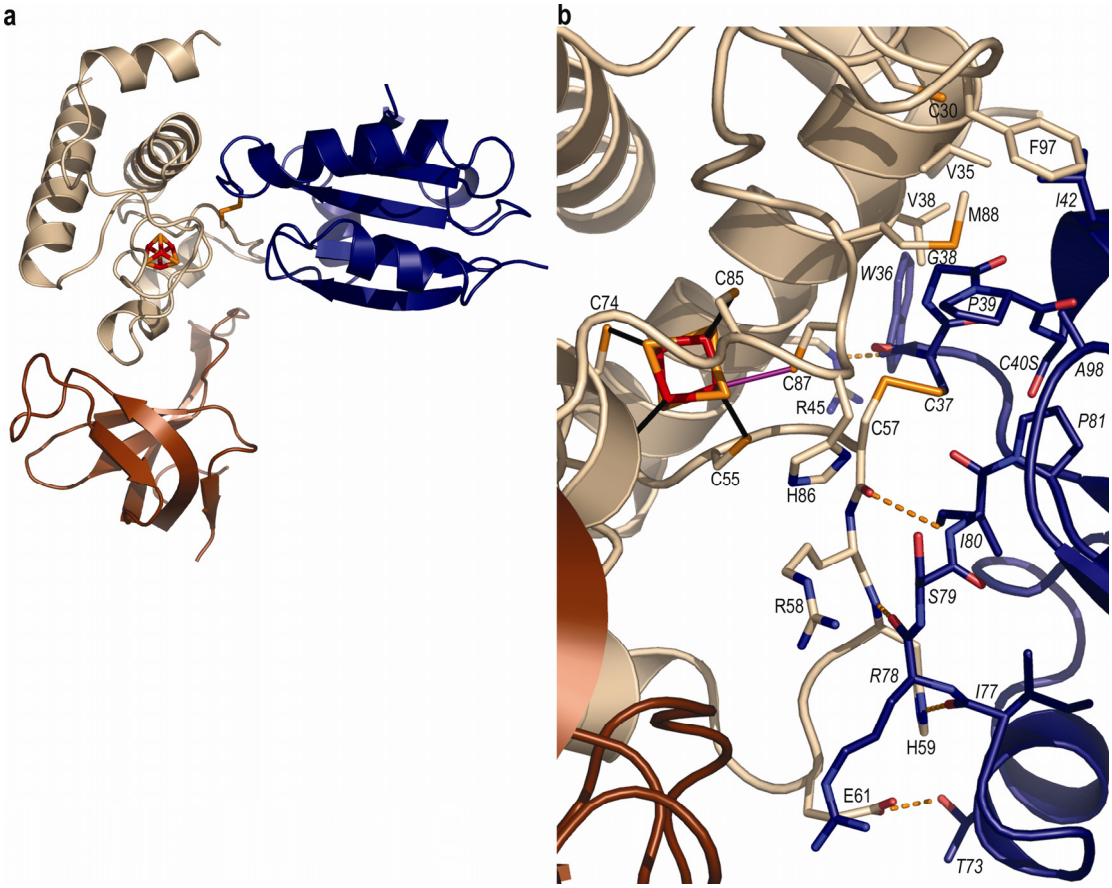

a) Overall structure of the FTR-Trx-*m* C40S complex. Trx-*m* C40S, catalytic and variable subunits of FTR are shown in blue, beige and brown, respectively. Trx-*m* exclusively interacts with the catalytic subunit of FTR.

b) The interactions between the catalytic subunit of FTR (beige) and Trx-*m* C40S (blue). An intermolecular disulfide bridge between Cys57 of FTR and Cys37 of Trx-*m* C40S, resembling the intermediate in the reaction, links the active sites of FTR and

the Trx. Hydrogen bonds are represented as orange dotted lines. Labels for amino acids in FTR and Trx are shown in regular and italics, respectively.

Supplementary Figure 5. FTR-Trx-*f* - FTR-Trx-*m* complex comparison.

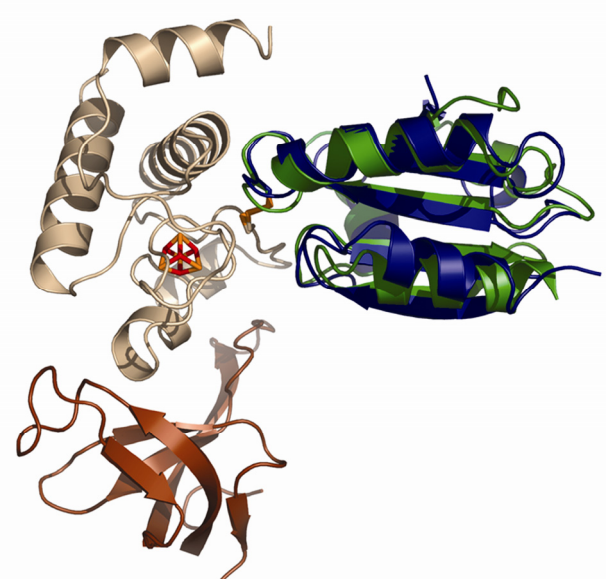

Superposition of the FTR-Trx-*f* C49S (Trx-*f* in green) and FTR-Trx-*m* C40S complexes (Trx-*m* in blue).

Supplementary Figure 6. Comparison of the interactions of the Trx-Reductase-Trx (TrxR-Trx), FTR-Trx-*f* and FTR-Trx-*m* complexes.

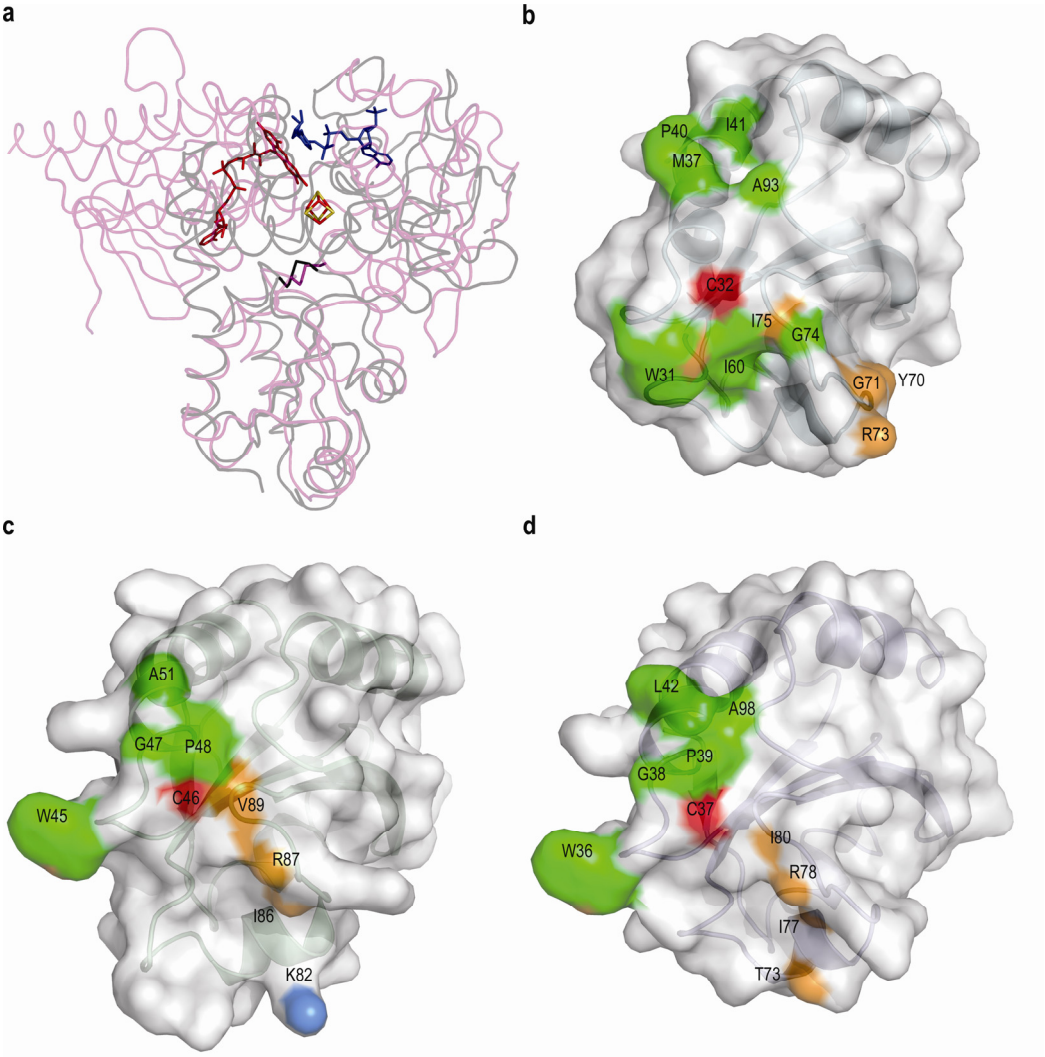

a) Superposition of *E. coli* TrxR-Trx complex[2] (light blue, pdb code: 1F6M) and FTR-Trx-*f* C49S (grey), where the Trxs are aligned (bottom part of figure). The [4Fe-4S] cluster (iron and sulphur atoms are coloured in red and orange, respectively) of FTR, FAD (red) and NADPH (blue) of TrxR and intermolecular

disulfide bridges are shown in sticks. The binding surface of FTR-Trx is smaller than that of TrxR-Trx.

b) Surface representation of the interaction area of Trx in the TrxR-Trx complex where all atoms that are involved forming hydrogen bonds, salt bridges, disulfide bridges or hydrophobic interactions with TrxR are coloured orange, blue, red and green, respectively.

c) Surface representation of the interaction area of Trx-*f* C49S in the FTR-Trx-*f* C49S complex. Colour coding as in b.

d) Surface representation of the interaction area of Trx-*m* C40S in the FTR-Trx-*m* C40S complex. Colour coding as in b.

Supplementary Figure 7. Comparison of binary complexes and ternary complex.

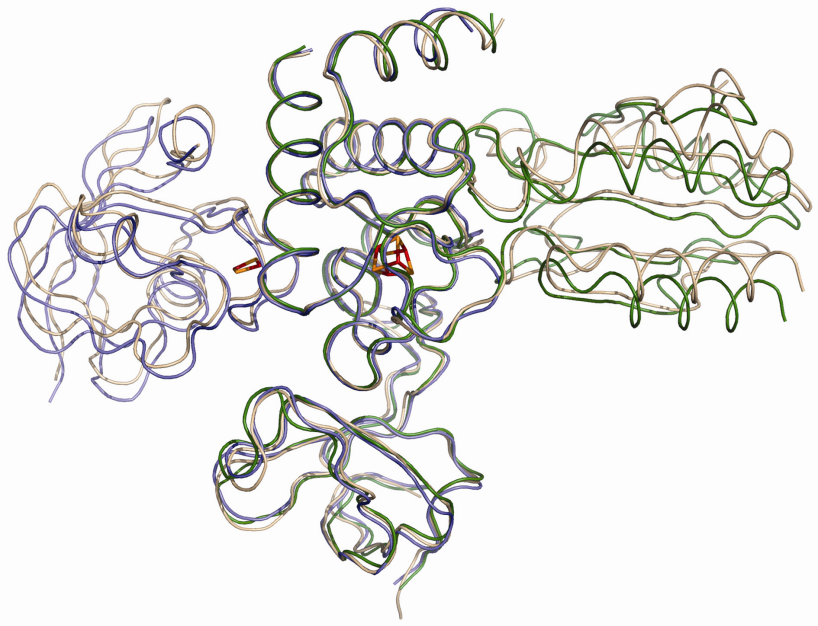

Superposition of Fdx-FTR-Trx-*f* (beige) FTR-Trx-*f* (green) and Fdx-FTR (blue) complexes.

Supplementary Figure 8. The different positions of His86 in resting, one-electron-reduced FTR and NEM-FTR, implying His86 plays an important role in reaction.

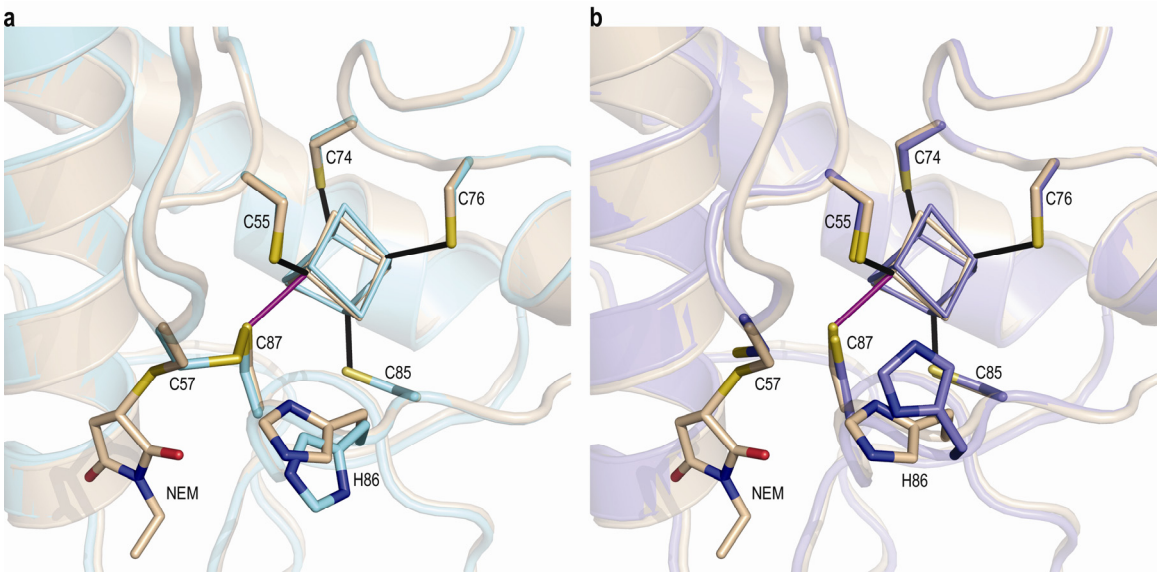

a) Superposition of the active sites of NEM-FTR (beige) and resting FTR (cyan). In NEM-FTR the disulfide bond is cleaved. Cys87 of NEM-FTR is ligated to an iron of the cluster (purple line), while Cys57 is bound to NEM. The imidazole ring of His86 moves towards Cys87 and the cluster from the resting state.

b) Superposition of the active sites of NEM-FTR (beige) and two-electron-reduced FTR (blue), showing highly similar orientations of Cys57 and Cys87. Both structures show that the reactive Cys57 can cleave the disulfide bridge of TRX. His86 is in van der Waals contacts with sulphur atoms of the cluster and Cys55, with distances of 3.5 Å and 3.7 Å respectively.

Supplementary Figure 9. Omit electron density map of the active-site disulfide and [4Fe-4S] cluster area of Fdx-FTR-Trx-*f* complex at 3.4 Å.

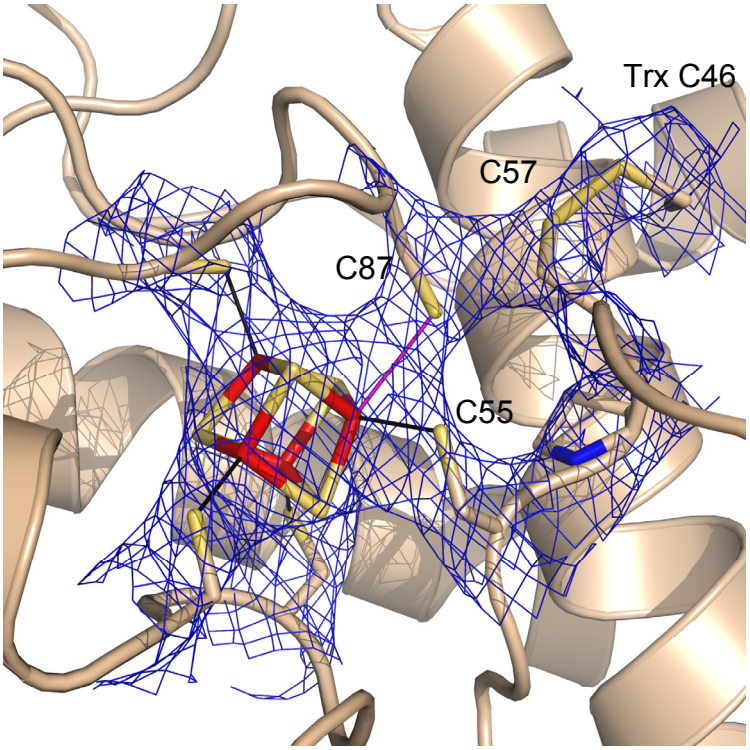

Simulated annealing $2F_o$-F_c omit electron map, where FTR Cys55, Cys57, Cys87 and the [4Fe-4S] cluster were omitted, contoured at 1σ. The [4Fe-4S] cluster of FTR is represented in sticks, where iron and sulphur atoms are coloured red and orange, respectively.

Supplementary Table 1. Data collection and refinement statistics

	Fdx-FTR	NEM-FTR	Two electron Reduced FTR
Data collection			
Beamline	SBC ID 19 APS	ALS BL8.2.1	SBC ID 19 APS
Space group	$C222_1$	$P2_12_12_1$	$P4_32_12$
Cell dimensions			
a, *b*, *c* (Å)	63.5, 89.7, 99.3	44.5, 53.5,79.3	45.1, 45.1, 172.4
α, β, γ (°)	90, 90, 90	90, 90, 90	90, 90, 90
Resolution (Å)	50 –2.4 (2.49-2.40)	50 –1.7 (1.76-1.70)	50 –1.95 (2.02-1.95)
R_{sym} or R_{merge}	8.4 (44.8)	6.1 (49.9)	5.9 (38.4)
$I/\sigma I$	30.4 (3.7)	29.2 (2.2)	22.00 (4.5)
Completeness (%)	95.7 (82.1)	93.9 (60.7)	93.1 (99.8)
Redundancy	5.3 (3.6)	6.6 (4.6)	4.8 (5.0)
Number of molecules in ASU[#]	1	1	1
Refinement			
Resolution (Å)	33.28-2.40	39.70-1.70	19.07-1.95
No. reflections	10877	20302	13061
R_{work}/ R_{free}	23.7/28.8	23.4/25.5	26.7/28.4
No. atoms			
Protein	2139	1453	1419
Iron-sulphur clusters	12	8	8
Water	108	93	77
B-factors			
Protein	56.7	40.9	47.0
Iron-sulphur clusters	48.5	27.0	32.5
Cys 55	43.8	30.7	37.7
Cys 74	34.6	26.2	33.8
Cys 76	31.6	24.4	32.4
Cys 85	40.6	29.2	36.6
Cys 87	46.1	32.5	40.8
Water	49.1	45.7	47.7
R.m.s deviations			
Bond lengths (Å)	0.006	0.005	0.006
Bond angles (°)	1.0	1.2	1.1
Ramachandran plot			
Most favoured region (%)	81.1%	88.8%	87.9%
Additional allowed region (%)	17.2%	11.2%	12.1%
Generously allowed region (%)	1.6%	0.0%	0.0%
Disallowed region (%)	0.0%	0.0%	0.0%

[#]ASU, an asymmetric unit

$R_{sym}=\Sigma_h\Sigma_i|I_{hi}-\langle I_h\rangle| / \Sigma_h\Sigma_i |I_{h,i}|$

R factor = $\Sigma||F_o|-|F_c|| / \Sigma|F_o|$, where F_o and F_c are observed and calculated structure factors, respectively

Continued

	FTR-Trx-*f* C49S*	Fdx-FTR-Trx-*f* C49S	FTR-Trx-*m* C40S
Data collection			
Beamline	In-house RaxisV	ALS BL8.2.1	ESRF, ID14-4
Space group	$P2_12_12_1$	$P3_221$	$P2_1$
Cell dimensions			
a, *b*, *c* (Å)	61.3, 66.8, 69.7	130.4, 130.4, 64.8	54.0, 42.2, 145.3
α, β, γ (°)	90, 90, 90	90, 90, 90	90, 90.3, 90
Resolution (Å)	50.0 –1.65 (1.71-1.65)	50-3.4 (3.52-3.40)	30-3.0 (3.16- 3.0)
R_{sym} or R_{merge}	7.0 (66.2)	13.4 (46.3)	10.0 (29.1)
$I/\sigma I$	44.8 (3.0)	11.5 (3.2)	12.1 (3.6)
Completeness (%)	95.6 (92.3)	99.5 (99.7)	99.8 (99.7)
Redundancy	14.1 (7.7)	12.6 (7.7)	3.6 (3.5)
Numbers. of molecules in ASU	1	1	2
Refinement			
Resolution (Å)	34.85-1.65	14.96 -3.40	30.0-3.0
No. reflections	33478	8467	13511
$R_{work/}$ R_{free}	20.8/22.7	20.2/26.4	23.5/28.4
No. atoms			
Protein	2335	3045	4563
Iron-sulphur clusters	8	12	16
Water	294	0	0
B-factors			
Protein	27.2	48.1	52.0
Iron-sulphur clusters	15.9	24.3	31.3
Cys 55 (FTR)	14.0	22.4	37.3
Cys 74 (FTR)	14.5	18.5	39.2
Cys 76 (FTR)	14.4	18.7	33.4
Cys 85 (FTR)	14.6	37.0	32.1
Cys 87 (FTR)	16.3	32.6	37.2
Water	36.4	N/A	N/A
R.m.s deviations			
Bond lengths (Å)	0.005	0.008	0.008
Bond angles (°)	1.2	1.3	1.5
Ramachandran plot			
Most favoured region (%)	87.7%	76.3%	85.1%
Additional allowed region (%)	11.5%	22.5%	14.1%
Generously allowed region (%)	0.8%	1.2%	0.6%
Disallowed region (%)	0.0%	0.0%	0.2%

* This data were merged from four crystals. All other data were collected on a single crystal.

Supplementary Table 2. Fe–S and S-S bond lengths of FTR [4Fe–4S] clusters

	Cys57 Sγ-Cys87 Sγ (Å)	Cys87 Sγ-Fe (Å)	Cys55 Sγ-Fe (Å)	Resolution (Å)	Oxidation State
Resting FTR[3]	2.05	3.14	2.38	1.6	2+
Fdx-FTR	2.04	3.15	2.32	2.4	2+
Two electron Reduced FTR	3.24	3.21	2.47	1.95	2+
NEM-FTR	3.52	2.72	2.55	1.7	3+
FTR-Trx-*f* C49S	2.96	2.84	2.45	1.65	3+
FTR-Trx-*m* C40S	3.61	2.94	2.45	3.0	3+
Fdx-FTR-Trx-*f* C49S	3.51	2.98	2.46	3.4	3+

References to supplementary materials

1. Kurisu, G. *et al.* Structure of the electron transfer complex between ferredoxin and ferredoxin-NADP(+) reductase. *Nat. Struct. Biol.* **8**, 117-121 (2001).
2. Lennon, B. W., Williams, C. H., Jr. & Ludwig, M. L. Twists in catalysis: alternating conformations of *Escherichia coli* thioredoxin reductase. *Science* **289**, 1190-1194 (2000).
3. Dai, S., Schwendtmayer, C., Schürmann, P., Ramaswamy, S. & Eklund, H. Redox signaling in chloroplasts: cleavage of disulfides by an iron-sulfur cluster. *Science* **287**, 655-658 (2000).